# Design and Analysis of Transitions from Rectangular Waveguide to Layered Ridge Dielectric Waveguide

George E. Ponchak, *Member, IEEE*, Nihad I. Dib, *Member, IEEE*, and Linda P. B. Katehi, *Fellow, IEEE*

***Abstract*— Transitions from rectangular waveguide to layered ridge dielectric waveguide are studied both experimentally and theoretically. In addition, a design procedure is given for each transition. The analysis and design procedures are valid for transitions between rectangular waveguide and other open dielectric waveguides such as image guide, insulated image guide, dielectric ridge guide, and inverted strip dielectric waveguide. It is shown that for small dielectric waveguides such as layered ridge dielectric waveguide, a transition which is comprised of a tapered ridge waveguide reduces the radiation loss by at least 1 dB.**

## I. Introduction

THERE has been a growing interest in the millimeter wave frequency spectrum for aircraft ground avoidance radars, intelligent vehicle highway systems, space debris tracking, intersatellite links, and missile tracking. In addition, both the millimeter and the submillimeter wave frequency spectra are required to detect most atmospheric constituents. The development of electronic components for the millimeter/submillimeter wave frequency spectrum is required for these applications.

For frequencies below 100 GHz, planar, quasi-TEM transmission lines such as microstrip and coplanar waveguide have been successfully used for monolithic amplifiers, mixers, and phase shifters. Although these planar, quasi-TEM type of transmission lines are highly suited for integrated circuits, the surface resistance increases with the square root of frequency [1]. In addition, the circuit dimensions must be decreased as the frequency is increased to maintain a single mode transmission line which further increases the conductor losses. The high attenuation makes microstrip and coplanar waveguide unsuitable for system integration or antenna feed networks in the millimeter and submillimeter wave frequency spectrum. Rectangular waveguide and other similar waveguides have low loss but are too large to effectively be used for many applications.

In recent years, a different class of transmission lines which do not require any conductors but instead use the difference in permittivities between two or more media to guide the electromagnetic energy have become popular. Examples of such dielectric waveguides are image guide [2], insulated image guide [3], trapped image guide [4], dielectric ridge guide [5], inverted strip dielectric waveguide [6], and layered ridge dielectric waveguide (LRDW) [7]. These dielectric waveguides have been used in antenna feed networks, frequency scannable antennas, radars, and oscillators.

As the use of dielectric waveguides increases, better transitions between rectangular waveguide and the dielectric waveguide will be required for integrating the circuits with test equipment and millimeter wave sources such as Gunn diodes which typically have a rectangular waveguide output port. The transitions must match the impedances of the two waveguides and transform the $TE_{10}$ mode of the rectangular waveguide to the propagating mode of the dielectric waveguide. The field transformation is especially difficult since the fields are well confined in the rectangular waveguide but only weakly confined in the dielectric waveguide. As the permittivity of the dielectric waveguide is increased or multiple layers of dielectrics are used to reduce the size of the dielectric waveguide, the field transformation is more difficult to accomplish.

This paper will present an analysis of four transitions from rectangular waveguide to LRDW and a design procedure which could be followed to optimize the transition design. Both experimental as well as the finite -difference time-domain (FDTD) method will be used in the transition analysis. The design procedure is based on the concept of the effective dielectric constant (EDC) method developed by McLevige [3]. Although the details of the analysis will be presented specifically for the LRDW, the methods and design procedures should be useful for other multilayer dielectric waveguides as well.

## II. Layered Ridge Dielectric Waveguide Description

LRDW consists of a strip comprised of two or more layers of dielectrics on a conductor backed dielectric substrate. The center dielectric layer has a lower permittivity than the substrate and top layer. Fig. 1 shows the LRDW line with the dimensions and dielectrics used throughout this paper. Although the LRDW can support both $E^x_{mn}$ and $E^y_{mn}$ modes, the $E^x_{11}$ mode has the lowest cutoff frequency and is therefore the dominant mode. Because of the continuity of the electric flux density across the dielectric boundaries for the $E^x_{11}$ mode, the electric field is stronger in the low permittivity layer which becomes the guiding layer in the low frequency region of the spectrum.

Manuscript received June 11, 1995; revised March 20, 1996. This work was supported by the Army Research Office (ARO) and the NASA/Lewis Research Center Director's Discretionary Fund.

G. E. Ponchak is with the NASA Lewis Research Center, Cleveland, OH 44135 USA.

N. I. Dib is with the Electrical Engineering Department at the Jordan University of Science and Technology, Irbid, Jordan.

L. P. B. Katehi is with the Electrical Engineering and Computer Systems Department, University of Michigan, Ann Arbor, MI USA.

Publisher Item Identifier S 0018-9480(96)04703-5.

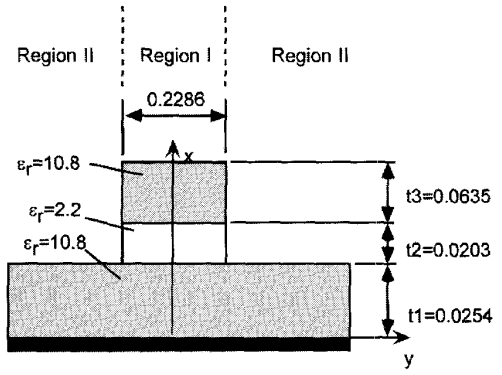


Fig. 1. Layered ridge dielectric waveguide for 26.5–40 GHz (dimensions in cm).

To design a transition between a rectangular waveguide and an LRDW, the fields of both waveguides must be known in order to visualize the necessary field transformation which must occur. It has been shown that the EDC method is useful for obtaining an engineering estimate of the propagation constant and the fields for many dielectric waveguides [2]–[5]. Since the method has been fully presented in the literature, only a brief outline as used in this paper will be given here. The EDC method uses the approximation that the LRDW may be separated and analyzed as two independent structures as shown in Fig. 2. Neither of these new structures has any variation along the $y$-axis and is therefore easier to solve. In general, the separation equation for Fig. 2 is given by

$$\begin{aligned} k_z^2 &= \epsilon_{ri} k_o^2 - k_{xi}^2 \\ &= \epsilon_{eq} k_o^2 \end{aligned} \tag{1}$$

where $i = 1$ to $N$ and $N$ is the total number of dielectric layers, $k_o = \omega\sqrt{\epsilon_o \mu_o}$, $k_{xi}$ is the separation variable for the $i$th layer, and

$$\epsilon_{eq} = \epsilon_{ri} - \left(\frac{k_{xi}}{k_o}\right)^2 \tag{2}$$

is referred to as the effective dielectric constant for the region. Note that $k_{xN} = jh_x$ is commonly used since the fields in the $N$th layer must be decaying to satisfy the radiation condition [1]. After $\epsilon_{eq}$ has been determined for each structure, the dielectric ridge can be replaced by the simple structure shown in Fig. 3. The separation equation for Fig. 3 is given by

$$\begin{aligned} k_z^2 &= \epsilon_{eq}^I k_o^2 - k_{y1}^2 \\ &= \epsilon_{eq}^{II} k_o^2 + h_y^2 \end{aligned} \tag{3}$$

which is used with the field equations to determine the propagation constant of the dielectric waveguide as given by

$$\epsilon_{eff} = \epsilon_{eq}^I - \left(\frac{k_{y1}}{k_o}\right)^2 \tag{4}$$

The fields for Fig. 2 may be written as a combination of LSM$^x$ and LSE$^x$ modes. Since the LSM$^x$ mode is dominant over the portion of the frequency spectrum which results in strong field confinement within the guiding layer, it is sufficient to consider only the LSM$^x$ mode in the analysis. Likewise, the structure of Fig. 3 can be solved as a sum of LSE$^y$ and LSM$^y$ modes, but since the fields derived in the analysis for Fig. 2 are primarily $E_x$ and $H_y$, the LSM$^y$ fields may be omitted.

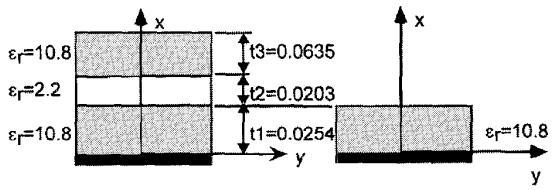


Fig. 2. Structures for analyzing the parameter $k_x$ using the EDC method where (a) represents region I, and (b) represents region II.

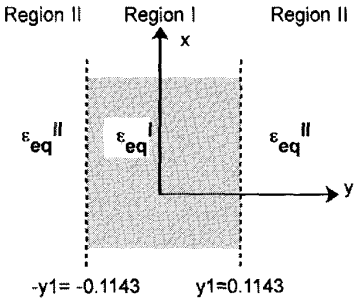


Fig. 3. Structure for analyzing the parameter $k_y$ using the EDC method.

## III. Transition Description

In the past, three types of transitions from rectangular waveguide to dielectric waveguide have been commonly used. These are shown in Fig. 4(a)–(c). In the first transition shown in Fig. 4(a), referred to as transition A in the rest of the paper, the dielectric waveguide is abruptly butted to the full height rectangular waveguide [8]. For larger dielectric waveguides such as image guide fabricated from low permittivity materials, this transition can give good results since the size of the image guide is comparable to the size of the rectangular waveguide. The second transition shown in Fig. 4(b) will be referred to as transition B in the rest of the paper. In transition B, the rectangular waveguide is transitioned to a reduced height rectangular waveguide so that there is greater field interaction between the rectangular waveguide and the dielectric waveguide. The rectangular waveguide may be made to be the same height as the dielectric waveguide but in practice, this is usually not done to allow for variations in the height of the dielectric waveguides. The most commonly used transition is shown in Fig. 4(c) and will be referred to as transition C in the rest of the paper. This transition adds a horn to transition B to convert the open dielectric waveguide to a shielded dielectric waveguide [9], [10]. A forth transition shown in Fig. 4(d), referred to as transition D in the rest of the paper, uses a tapered ridge waveguide to concentrate the power of the rectangular waveguide to the region of the dielectric waveguide. The ridge is then continued into the horn to provide a smooth match to the open dielectric waveguide

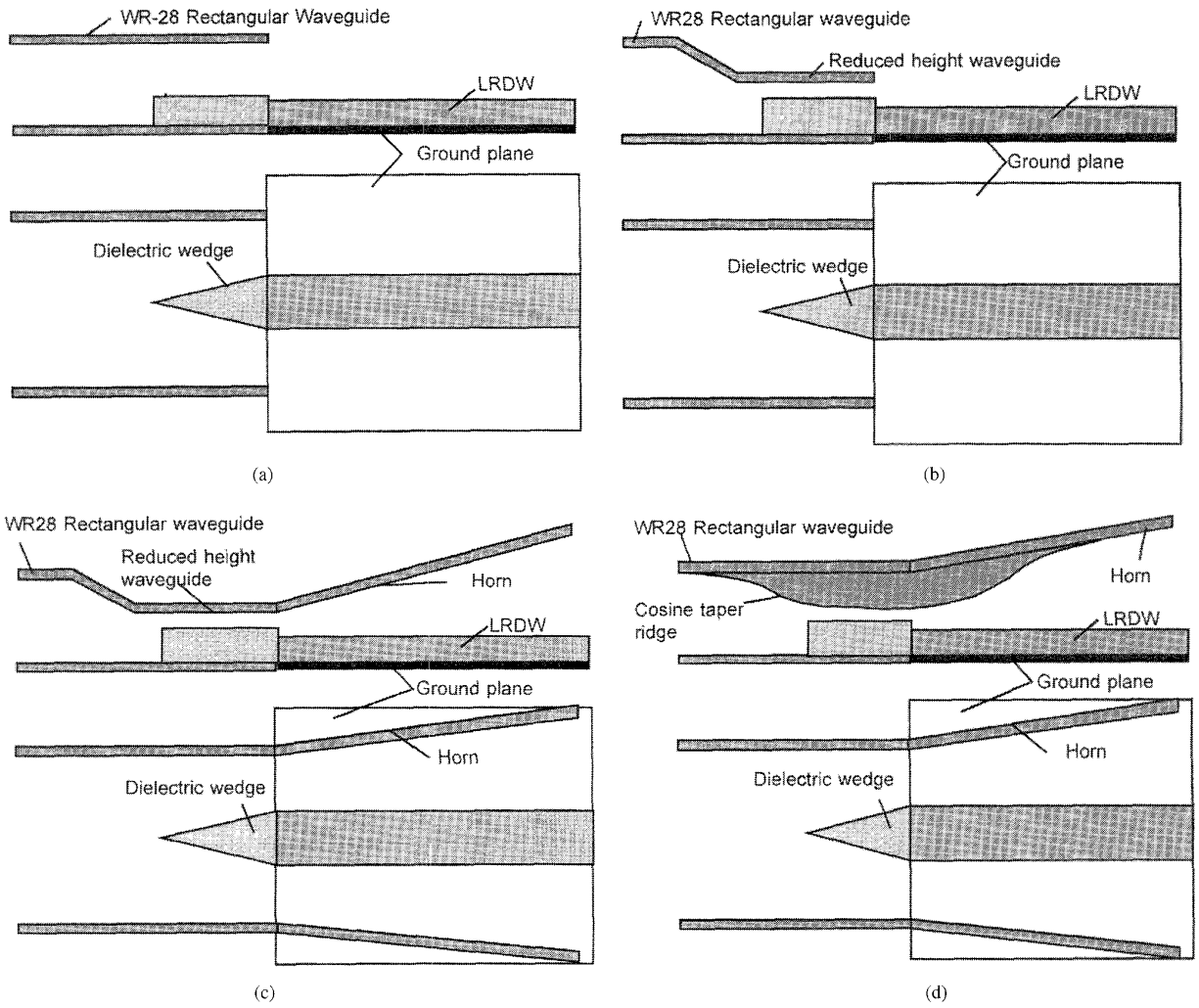


Fig. 4. Transitions from rectangular waveguide to layered ridge dielectric waveguide where (a), (b), (c), and (d) shows transitions A, B, C, and D, respectively.

[11], [12]. The ridge may be made to contact the dielectric waveguide. In each of these transitions, a dielectric wedge may be used to create the field transformation [13] or to improve the impedance match of the transition [14]. When the dielectric wedge is used for providing the field transformation, it must be 3–5 $\lambda_g$ long.

## IV. Transition Analysis Using Finite-Difference Time-Domain

The FDTD method is well known [16] and thus will not be presented here. The excitation mechanism used in this research is similar to that described in [17], [18]. To approximate the $TE_{10}$ mode, the amplitude of the incident field has a half wavelength sinusoidal distribution across the rectangular guide in the y-direction and is uniform in the $x$-direction. Moreover, the incident field has a spatial variation in the $z$-direction given by a Gaussian envelope imposed on a sinusoidally varying carrier. The super-absorbing first-order Mur boundary condition [19] is used at the front and back walls of the computational domain in order to simulate infinitely long lines. Numerical experiments have shown that such an absorbing boundary condition (ABC) reduces reflections appreciably compared to, for example, first-order Mur without the super-absorber [14]. The above ABC's require a choice for the incident velocity of the waves, or equivalently $\epsilon_{eff}$. At the front wall, an $\epsilon_{eff}$ that corresponds to the velocity of the waves in an empty waveguide, at a frequency which is approximately at the middle of the frequency range of interest, is chosen. On the other hand, at the back wall, an $\epsilon_{eff}$ that corresponds to the velocity of the waves in the LRDW is chosen. An estimate of this latter $\epsilon_{eff}$ may be obtained using the compact 2-D–FDTD technique [20], [21] or the mode matching technique [7]. It should be mentioned that the above choice of $\epsilon_{eff}$ assumes that only the propagating dominant mode exists in the dielectric waveguide. The first-order Mur boundary condition was used on the top and side walls surrounding the LRDW in order to simulate an open structure.

## V. Experimental Characterization of Transitions

The LRDW was fabricated from RT/Duroid$^{TM}$ 5880 and 6010 substrates which have relative permittivities of 2.2 and

10.8, respectively. Rogers$^{TM}$ 3001 bonding film was used to glue the substrates together. The transitions were characterized using an HP8510B Vector Network Analyzer with a WR-28 Reflection/Transmission test set. The system was calibrated using an open-short-load calibration procedure. For the through measurements, two transitions were connected back to back through a 19 cm long section of LRDW. The same LRDW was used for all of the measurements so that comparisons between transitions could be made. For the return loss measurements, microwave absorbing material was placed over the LRDW to eliminate power returned from the second transition. Before each set of data was taken, the time domain option of the HP8510 was used to verify that all of the reflections were due to the transitions and not because of fabrication imperfections in the LRDW. To fabricate the dielectric wedges, RT/Duroid$^{TM}$ 5880, 6010, and 6006 which has a dielectric constant of 6.0 were used. Standard microwave substrate thicknesses in the range of 0.0254–0.157 cm were used.

## VI. Transition Analysis Using TLIN Method

The analysis of many microwave circuit problems may be greatly simplified through the use of transmission line theory (TLIN) and wave impedances. In general, wave impedances are defined as the ratio of the transverse field components which give rise to power flow along a mutually perpendicular axis. For transverse electric modes, the wave impedance may be written in the general form

$$Z = \frac{k_o \eta_o}{k_z} \tag{5}$$

which translates to

$$Z = \frac{\eta_o}{\sqrt{\epsilon_{eff} - \left(\frac{\lambda_o}{\lambda_c}\right)^2}} \tag{6}$$

for perfectly conducting cylindrical waveguides and to

$$Z = \frac{\eta_o}{\sqrt{\epsilon_{eff}}} \tag{7}$$

for open dielectric waveguides. The parameters in (5)–(7) are $\eta_o = \sqrt{\mu_o/\epsilon_o}$ is the free space impedance, $\lambda_o$ is the free space wavelength, $\epsilon_{eff}$ is the effective permittivity of the medium filling the waveguide, and $\lambda_c$ is the cutoff wavelength of the empty cylindrical waveguide.

Although it is possible to take a large number of cross sectional cuts through the transition, determine the wave impedance at each plane, and calculate the reflection coefficient very accurately, a good engineering estimate of the reflection coefficient may be obtained if only the most significant impedance mismatches are used. Fig. 5 shows a time domain plot of $S_{11}$ for transition D measured on the HP8510B. The markers are positioned at three reflection points along the transition. Marker 1 is at the start of the LRDW under the ridge, Marker 2 is at a point inside the horn, and Marker 3 is at the end of the horn. It is clear that the reflection from the start of the LRDW is far larger than any other reflection

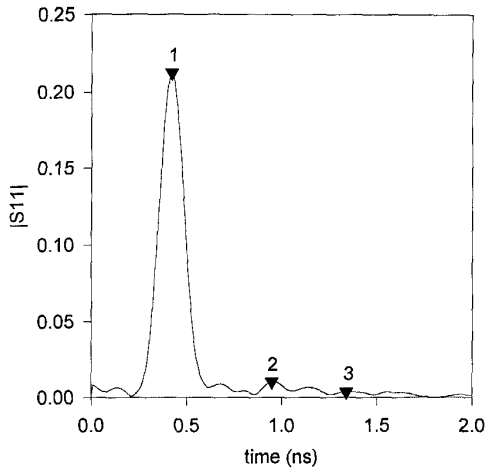


Fig. 5. Measured time domain $S_{11}$ for transition D with no matching wedge.

and for an engineering estimate of the reflection coefficient for the transition, all other parts of the transition may be omitted. Using these assumptions, the transitions may be analyzed using the TLIN method at the single discontinuity which results in the simple equation

$$\Gamma = \frac{Z^w - Z^d}{Z^w + Z^d} \tag{8}$$

where $Z^w$ is the wave impedance of the rectangular or ridged waveguide and $Z^d$ is the wave impedance of the open or shielded dielectric waveguide. The $\epsilon_{eff}$ of the dielectric guides and the partially filled rectangular waveguides were determined from the EDC method. The cutoff wavelengths of the ridge waveguides were calculated using Hoefer's equations [15].

## VII. Results

To verify the accuracy of the TLIN and the FDTD methods of analysis, $|S_{11}|$ has been plotted for all of the transitions in Fig. 6. Several observations are made. First, the measured return loss is lower than that predicted by the TLIN and the FDTD methods. This is expected since the FDTD method does not take into account the conductor and dielectric losses, whereas the TLIN method assumes a completely lossless junction. Second, except for transition A, the agreement between the theoretically predicted loss (using the TLIN and the FDTD) and the measured return loss is satisfactory. In each case, the three methods yield a return loss within $\pm 3$ dB of each other. Furthermore, the TLIN method and the FDTD method are generally within $\pm 1.5$ dB of each other. The FDTD analysis was not performed for transition A. Also, for transition A, the TLIN method is not in agreement with the measurements because of the small field overlap between the two waveguides which makes the TLIN method less accurate.

Fig. 7 shows the measured insertion loss for transitions A, C, and D. The insertion loss of transitions B and C is approximately the same across the band with the exception of the higher frequency part of the band when a resonance is noted in transition C. Transition A has a greater insertion loss

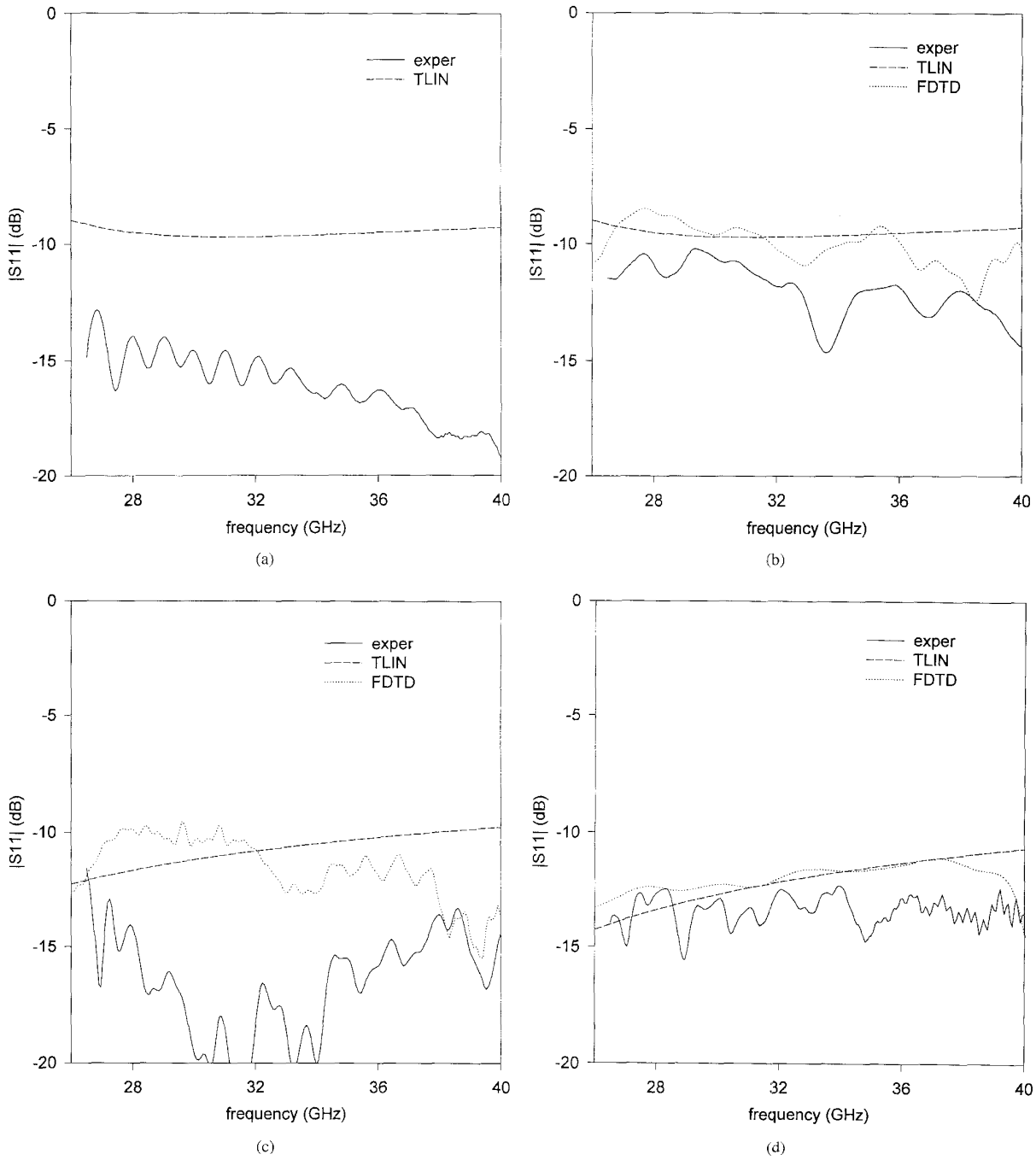


Fig. 6. Measured and calculated return loss for transitions A, B, C, and D in (a), (b), (c), and (d), respectively.

than the other transitions and the insertion loss of transition D is at least 2 dB less than the other transitions. When the loss factor, $1 - |S_{11}|^2 - |S_{21}|^2$, is calculated for each of the transitions, it is noted that transition D has the lowest loss factor while transition A has the greatest loss factor. Since ridge waveguide has higher conductor loss than rectangular waveguide, it follows that transition D has the lowest radiation loss of the four transitions; at least 1 dB per transition lower than transition C. Also, it may be stated that minimizing the return loss alone is not a valid design criteria for open transitions. Although transitions A and C had the lowest measured return loss, they also had the highest radiation loss which makes them undesirable for transitions to antenna feed networks or other applications where crosstalk must be minimized.

Resonances in the insertion loss plots for transitions C and D at the higher frequencies are seen in Fig. 7. By correlating the onset frequency of the resonances with the cutoff frequencies

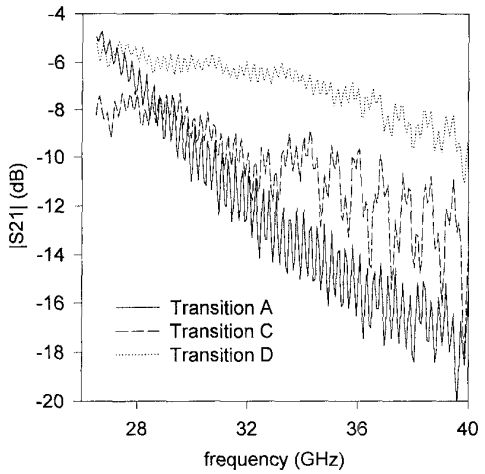


Fig. 7. Measured insertion loss of transitions A, C, and D without a dielectric matching wedge.

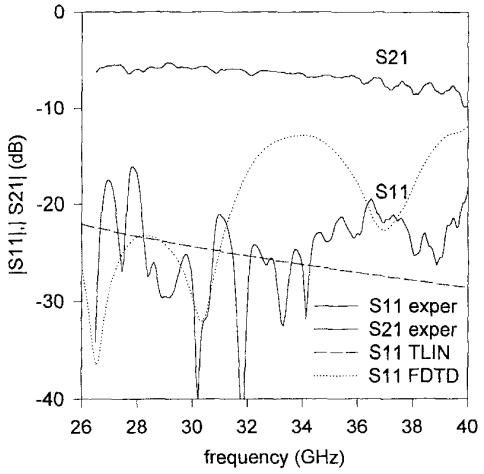


Fig. 8. Measured and calculated characteristics of transition D with a dielectric matching wedge.

of the higher order rectangular waveguide modes in the horn and with the field plots for both the LRDW and the rectangular waveguide, it has been determined that the resonances are due to the $TE_{31}$ mode in the rectangular horn. Reducing the width of the horn shifts the onset frequency of the resonances to higher frequencies and may be used to eliminate them from the waveguide band. A slight degradation in $S_{11}$ would be expected if this were done. Note the 2–3 dB degradation in $|S_{11}|$ between Fig. 6(b) which has no horn and Fig. 6(c) which has a horn.

To provide impedance matching between the rectangular waveguide and the LRDW, dielectric wedges were added to the transitions. For Image Guide and other single material dielectric waveguides, the dielectric wedges are typically constructed from the same material as the guiding layer of the dielectric waveguide [13], [14]. For layered dielectric waveguides, this is not practical. To determine the optimum wedge material, thickness, and length for the LRDW, the characteristics of each transition was experimentally characterized for many matching wedges. It was determined that for transitions B, C, and D, a dielectric wedge with a relative permittivity of 6.0, a thickness of 0.127 cm, and a length of 1.91 cm provided optimum return loss. Although longer wedges tended to reduce the return loss, they also created resonances in the $|S_{21}|$ characteristics due to reflections between the two ends of the wedge. This was easily seen using the time domain option of the HP8510B ANA.

The use of the matching wedge greatly improved the measured characteristics of each transition. Fig. 8 shows the measured as well as the calculated return loss and the measured insertion loss of transition D with the experimentally determined optimum matching wedge. Note that the return loss is typically 20 dB compared to the 14 dB without the wedge. Also, the high frequency noise seen on the insertion loss plots of Fig. 7 have been eliminated. Table I summarizes the measured performance of each transition. In Table I, the worst case return loss value across the waveguide band is given. Transition D has the lowest insertion loss and the best return loss. Also, there is a significant improvement in the characteristics of transitions B and C with the addition of the dielectric wedge. In these two transitions, the dielectric wedge not only provides impedance matching but is also the only means of transforming the fields of the two different waveguides.

TABLE I
SUMMARY OF MEASURED TRANSITIONS PERFORMANCE

| Transition type | $S_{11}$ (dB) | $S_{21}$ at 26.5 GHz (dB) | $S_{21}$ at 40.0 GHz (dB) |
|---|---|---|---|
| A, no wedge | 12.8 | 5.0 | 18.0 |
| B, no wedge | 10.2 | 9.0 | 12.0 |
| B, with wedge | 12.3 | 5.5 | 10.0 |
| C, no wedge | 11.6 | 8.0 | 13.0 |
| C, with wedge | 16.0 | 4.8 | 10.5 |
| D, no wedge | 12.3 | 5.5 | 10.0 |
| D, with wedge | 16.2 | 5.5 | 8.2 |

To gain a better understanding of the transition, the FDTD method was used to obtain electric field along the center of the waveguide for transitions C and D without a matching wedge. These are shown in Fig. 9(a) and (b), respectively. The transmitted wave is approximately at the same location in each figure. Notice that the power transitioned to the LRDW is confined in the low dielectric layer. Furthermore, this guided signal in the LRDW lags the radiated power emerging from the horn as expected. The radiated power is especially evident in Fig. 9(a) where the plane wave emerging from the horn is easily seen. Comparing the two figures, it is seen that transition D has a smaller radiated signal than transition C. In fact, although the pulse in Fig. 9(b) is slightly ahead of the pulse in Fig. 9(a), no radiated plane wave is apparent.

## VIII. DESIGN GUIDELINES

The data presented shows the advantage of using a flared horn on the output of the transition to better match the shielded

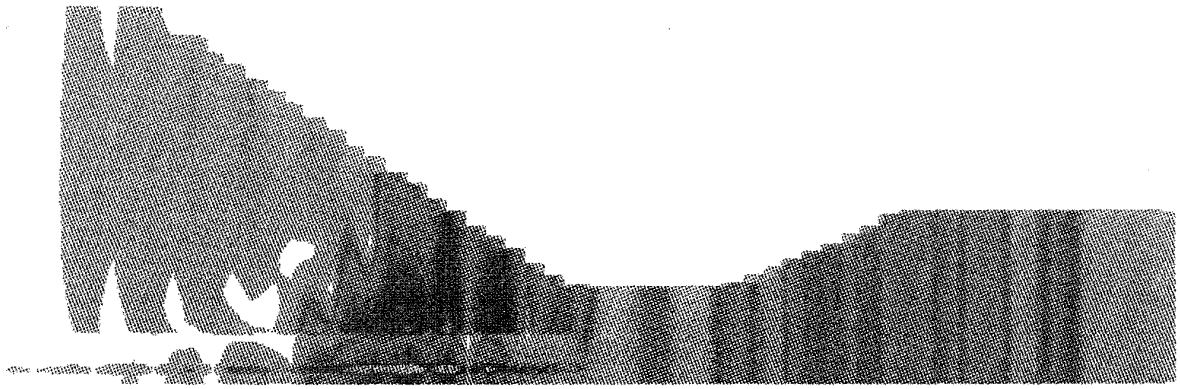

(a)

(b)

Fig. 9. Electric field along the center of the waveguide at 33 GHz without a dielectric wedge calculated using FDTD method. (a) Transition C and (b) transition D.

LRDW to the open LRDW. The data has also shown that the width of the horn must be controlled to eliminate the $TE_{31}$ mode which couples to the LRDW and creates resonances. Furthermore, it has been shown that a dielectric wedge may be used to greatly improve the return loss characteristics of the transitions. Lastly, it has been shown in Figs. 6 and 8 that the EDC method can accurately be used to calculate the return loss of the transitions. It is therefore reasonable to use the EDC method as a design aid.

In this section, the EDC method will be used to optimize the dielectric matching wedge parameters. From TLIN theory, the return loss is minimized when the wave impedances of the two waveguides are equal. For transitions A and B where the LRDW is unshielded, this translates to the condition

$$\frac{\eta_o}{\sqrt{\epsilon^{\mathrm{LRDW}}}} = \frac{\eta_o}{\sqrt{\epsilon^w - \left(\frac{\lambda_o}{\lambda_c^w}\right)^2}} \tag{9}$$

and for transitions C and D where the LRDW is shielded the matching condition is

$$\frac{\eta_o}{\sqrt{\epsilon^{\mathrm{LRDW}} - \left(\frac{\lambda_o}{\lambda_c^{\mathrm{LRDW}}}\right)^2}} = \frac{\eta_o}{\sqrt{\epsilon^w - \left(\frac{\lambda_o}{\lambda_c^w}\right)^2}} \tag{10}$$

where $\epsilon^{\mathrm{LRDW}}$ is the effective dielectric constant of the LRDW, $\epsilon^w$ is the effective dielectric constant of the partially filled rectangular waveguide or ridged waveguide containing the dielectric matching wedge, and $\lambda_c^{\mathrm{LRDW}}$ and $\lambda_c^w$ are the cutoff wavelengths of the empty rectangular waveguide or ridged waveguide housing the LRDW and the dielectric wedge, respectively. Equations (9) and (10) may be simplified to

$$\epsilon^w = \epsilon^{\mathrm{LRDW}} + \left(\frac{\lambda_o}{\lambda_c^w}\right)^2 \tag{11}$$

and

$$\epsilon^w = \epsilon^{\mathrm{LRDW}} - \left(\frac{\lambda_o}{\lambda_c^{\mathrm{LRDW}}}\right)^2 + \left(\frac{\lambda_o}{\lambda_c^w}\right)^2 \tag{12}$$

respectively. If the LRDW is in the same waveguide as the dielectric wedge, then $\lambda_c^{\mathrm{LRDW}} = \lambda_c^w$ and (12) simply states that the effective permittivities of the two waveguides must be matched. Since all of the terms on the right hand side of (11) and (12) are known, $\epsilon^w$ may be determined.

The design will proceed for transitions C and D although the relevant equations may be replaced to optimize transitions A and B. Start with the eigenvalue equation for the determination of the parameter $k_y$. For the LRDW in the transition, a

magnetic wall exists along the $x$-axis and an electric wall at $y_2$ must be used to represent the side walls of the rectangular waveguide. The resulting equation is

$$k_{y1} \tan(k_{y1} y_1) - k_{y2} \cot[k_{y2}(y_2 - y_1)] = 0 \tag{13}$$

where

$$k_{y1} = k_o \sqrt{\epsilon_{eq}^I - \epsilon^w}$$
$$k_{y2} = k_o \sqrt{1 - \epsilon^w} \tag{14}$$

and $\epsilon_{eq}^I$ is the equivalent dielectric constant for the region of the guide containing the dielectric wedge and $y_1$ is equal to one half of the wedge width. In (14), the assumption that $\epsilon_{eq}^{II} = 1$ was used. For most cases, this is valid since the substrate is generally very thin to suppress surface wave modes which would cause power leakage. $\epsilon_{eq}^I$ may be obtained through the solution of (13) with (14) and the assumption that the width of the wedge and the LRDW are equal.

Knowing $\epsilon_{eq}^I$, it is possible to solve for the permittivity of the dielectric wedge, $\epsilon_{r1}$, as a function of the wedge thickness, $t_1$, using the eigenvalue equation for the parameter $k_x$. For the case of two dielectric regions bound by perfect conductors, the eigenvalue equation is

$$\frac{k_{x1}}{\epsilon_{r1}} \tan(k_{x1} t_1) + k_{x2} \tan[k_{x2}(x_2 - t_1)] = 0 \tag{15}$$

where

$$k_{x1} = k_o \sqrt{\epsilon_{r1}^I - \epsilon_{eq}^I}$$
$$k_{x2} = k_o \sqrt{1 - \epsilon_{eq}^I} \tag{16}$$

and $x_2$ is the total height of the shield.

The solution of (15) and (16) results in a set of permittivities and thicknesses for the dielectric wedge which are each optimized according to the TLIN method. The task now is to choose the optimum combination from this set of solutions. The equalization of wave impedances is not sufficient if there is little field overlap between the two waveguides. This was seen in Fig. 6(a) which is the return loss for transition A. It is also necessary to optimize the field match between the two waveguides. This can be accomplished through a mode matching analysis [22]. If the analysis is simplified to use only the dominant mode in each waveguide, the reflection coefficient is given by

$$\Gamma = \frac{I_{11} I_{11}' - I_1 I_1'}{I_{11} I_{11}' + I_1 I_1'} \tag{17}$$

where

$$I_1 = \int_0^a [E^w(x)]^2 \, dx$$
$$I_1' = \int_0^{a'} [H^{\mathrm{LRDW}}(x)]^2 \, dx$$
$$I_{11} = \int_0^a E^w(x) E^{\mathrm{LRDW}}(x) \, dx$$
$$I_{11}' = \int_0^{a'} H^w(x) H^{\mathrm{LRDW}}(x) \, dx \tag{18}$$

and $a$ and $a'$ are the height of the two waveguides. The field components can be obtained from the EDC analysis. As a further simplification, the fields are taken for the case equivalent to Fig. 2(a). This is justified since most of the energy is confined at the center of the LRDW, the center of the ridge waveguide, and the center of the reduced height rectangular waveguide when the dielectric wedge is present. It is a simple procedure to solve (17) for each of the possible wedge combinations obtained from the TLIN analysis.

When this procedure was performed for the transitions C and D, it was found that the optimum wedge parameters are $\epsilon_r = 7.0$ with a thickness of 0.107 cm and $\epsilon_r = 6.0$ with a thickness of 0.112 cm, respectively. Note that this is very close to the optimum wedge parameters of $\epsilon_r = 6.0$ and a thickness of 0.127 cm found experimentally where only standard substrate permittivities and thicknesses could be used. Furthermore, the optimum wedge thickness corresponds to the thickness of the LRDW for the cases presented. Although this may not be true for all dielectric waveguides and for all frequencies, a first order design of the wedge may be obtained by using (11)–(16) with that assumption.

## IX. Conclusion

Four transitions were analyzed using a transmission line (TLIN) analysis, an FDTD, and experimentally, it has been shown that the FDTD analysis accurately models the transitions. In addition, it was shown that the TLIN method gave acceptable results. Using the effective dielectric constant and the TLIN methods, a simple design procedure was given for the transition design and the design of the dielectric matching wedge. For small sized dielectric waveguides such as LRDW, a transition comprised of a tapered ridge waveguide reduced the radiation loss of the transition by approximately 1 dB while simultaneously having an excellent return loss.

## References


[1] R. E. Collin, *Foundation for Microwave Engineering.* New York: McGraw-Hill Book Co., 1966.

[2] R. M. Knox and P. P. Toulios, "Integrated circuits for the millimeter through the optical frequency range," in *Proc. Symp. Submillimeter Waves,* New York, Mar. 31–Apr. 12, 1970, pp. 497–516.

[3] W. V. McLevige, T. Itoh, and R. Mittra, "New waveguide structures for millimeter-wave and optical integrated circuits," *IEEE Trans. Microwave Theory Tech.,* pp. 788–794, Oct. 1975.

[4] T. Itoh and B. Adelseck, "Trapped image guide for millimeter-wave circuits," *IEEE Trans. Microwave Theory Tech.,* pp. 1433–1436, Dec. 1980.

[5] T. Wang and S. E. Schwarz, "Design of dielectric ridge waveguides for millimeter-wave integrated circuits," *IEEE Trans. Microwave Theory Tech.,* pp. 128–134, Feb. 1983.

[6] T. Itoh, "Inverted strip dielectric waveguide for millimeter-wave integrated circuits," *IEEE Trans. Microwave Theory Tech.,* pp. 821–827, Nov. 1976.

[7] A. G. Engel, Jr. and L. P. B. Katehi, "Low-loss monolithic transmission lines for submillimeter and terahertz frequency applications," *IEEE Trans. Microwave Theory Tech.,* pp. 1847–1854, Nov. 1991.

[8] K. Solbach, "Electric probe measurements on dielectric image lines in the frequency range of 26–90 GHz," *IEEE Trans. Microwave Theory Tech.,* pp. 755–758, Oct. 1978.

[9] A. K. Tiwari and R. P. Singh, "An efficient image guide mode launcher," *Int. J. Infrared and Millimeter Waves,* vol. 7, no. 6, pp. 845–856, 1986.

[10] M. Dydyk, "Image guide: A promising medium for EHF circuits," *Microwaves,* pp. 71–80, Apr. 1981.

[11] T. H. Oxley and P. L. Lowbridge, "Image guide and microstrip integrated W-band receivers," *Microwave J.,* pp. 117–136, Nov. 1983.

[12] G. E. Ponchak, N. I. Dib, and L. P. B. Katehi, "A novel transition between rectangular waveguide and layered ridge dielectric waveguide," in *Proc. 24th European Microwave Conf.*, Cannes, France, Sept. 5–8, 1994, pp. 1933–1937.
[13] S. A. Pogarsky and I. I. Saprykin, "Resonant phenomena in hybrid structures," *Int. J. Infrared and Millimeter Waves*, vol. 15, no. 7, pp. 1325–1333, 1994.
[14] N. I. Dib and L. P. B. Katehi, "Analysis of the transition from rectangular waveguide to shielded dielectric image guide using the finite-difference time-domain method," *IEEE Microwave Guided Wave Lett.*, pp. 327–329, Sept. 1993.
[15] W. J. R. Hoefer and M. N. Burton, "Closed-form expressions for the parameters of finned and ridged waveguides," *IEEE Trans. Microwave Theory Tech.*, pp. 2190–2194, Dec. 1982.
[16] K. Kunz and R. Luebbers, *The Finite Difference Time Domain Method for Electromagnetics*. Florida: CRC Press, 1993.
[17] P. Alinikula and K. Kunz, "Analysis of waveguide aperture coupling using the finite-difference time-domain method," *IEEE Microwave Guided Wave Lett.*, vol. 1, pp. 189–191, Aug. 1991.
[18] M. De Pourcq, "Field and power-density calculations in closed microwave systems by 3-D finite differences," in *IEE Proc.*, vol. 132, pt. H, no. 6, pp. 360–368, Oct. 1985.
[19] K. Mei and J. Fang, "Superabsorption—A method to improve absorbing boundary conditions," *IEEE Trans. Antennas Propagat.*, vol. 40, pp. 1001–1010, Sept. 1992.
[20] A. Asi and L. Shafai, "Dispersion analysis of anisotropic inhomogeneous waveguides using compact 2-D–FDTD," *Electronics Lett.*, vol. 28, no. 15, pp. 1451–1452, July 1992.
[21] N. Dib and L. Katehi, "Dispersion analysis of multilayer planar lines containing Ferrite regions using an extended 2-D–FDTD method," in *1993 AP-S Symp. Dig.*, Ann Arbor, MI, June 1993, pp. 842–845.
[22] D. M. Pozar, *Microwave Engineering*. New York: Addison-Wesley, 1990.

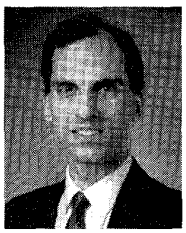

**George E. Ponchak** (S'82–M'90) received the B.E.E. degree from Cleveland State University in 1983 and the M.S.E.E. degree from Case Western Reserve University in 1987. He is currently pursuing the Ph.D. degree in electrical engineering from the University of Michigan.

He joined NASA Lewis Research Center in July, 1983. Since joining NASA, he has been responsible for the characterization and development of microwave/millimeter wave printed transmission lines, passive circuits, and multilayer interconnect technologies, the management of MMIC contracts, and the development of a NASA GaAs MMIC Reliability Assurance Guide.

**Nihad I. Dib** (S'89–M'92) received the B.Sc. and M.Sc. degrees in electrical engineering from Kuwait University in 1985 and 1987, respectively, and the Ph.D. in electrical engineering from the University of Michigan, Ann Arbor, in 1992.

From 1993 to 1995, he was an Assistant Research Scientist at the Radiation Laboratory at the University of Michigan, Ann Arbor. In 1995, he joined the Electrical Engineering Department at the Jordan University of Science and Technology as an Assistant Professor. His interests include the numerical analysis and modeling of planar discontinuities and dielectric lines.

**Linda P. B. Katehi** (S'81–M'84–SM'89–F'95) received the B.S.E.E. degree from the National Technical University of Athens, Greece, in 1977, and the M.S.E.E. and Ph.D. degrees from the University of California, Los Angeles, in 1981 and 1984, respectively.

In September 1984, she joined the faculty of the EECS Department of the University of Michigan, Ann Arbor. Since then, she has been interested in the development and characterization (theoretical and experimental) of microwave, millimeter-wave printed circuits, the computer-aided design of VLSI interconnects, the development and characterization of micromachined circuits for millimeter-wave and submillimeter-wave applications, and the development of low-loss lines for Terahertz-frequency applications. She has also been studying theoretically and experimentally various types of uniplanar radiating structures for hybrid-monolithic oscillator and mixer designs. She has been the author and co-author of more than 220 papers published in referred journals and symposia proceedings.

She has been awarded with the IEEE AP-S W. P. King (Best Paper Award for a Young Engineer) in 1984, the IEEE AP-S S. A. Schelkunoff Award (Best Paper Award) in 1985, the NSF Presidential Young Investigator Award and an URSI Young Scientist Fellowship in 1987, the Humboldt Research Award, and The University of Michigan Faculty Recognition Award in 1994, and the IEEE MTT-S Microwave Prize in 1996. She is a member of IEEE AP-S, MTT-S, Sigma XI, Hybrid Microelectronics, URSI Commission D, and a member of AP-S ADCOM from 1992 to 1995. Also, Dr. Katehi is an Associate Editor for the IEEE TRANSACTIONS ON ANTENNAS AND PROPAGATION and IEEE TRANSACTIONS ON MICROWAVE THEORY AND TECHNIQUES. She has graduated 11 Ph.D. students and is currently supervising 15 Ph.D. graduate students.